



# Using Clumped Isotopes to Reconstruct the Maximum Burial Temperature: A Case Study in the Sichuan Basin

Pingping Li<sup>1,2\*</sup>, Jinbao Duan<sup>3</sup>, Zhongzhen Cheng<sup>2</sup> and Huayao Zou<sup>1,2</sup>

<sup>1</sup>State Key Laboratory of Petroleum Resources and Prospecting, China University of Petroleum, Beijing, China, <sup>2</sup>College of Geosciences, China University of Petroleum, Beijing, China, <sup>3</sup>SINOPEC Exploration Company, Chengdu, China

## OPEN ACCESS

### Edited by:

Qiangtai Huang,  
Sun Yat-sen University, China

### Reviewed by:

Jibao Dong,  
Institute of Earth Environment (CAS),  
China

Fuyun Cong,  
China University of Geosciences  
Wuhan, China

### \*Correspondence:

Pingping Li  
lpp@cup.edu.cn

### Specialty section:

This article was submitted to  
Geochemistry,  
a section of the journal  
Frontiers in Earth Science

**Received:** 16 August 2021

**Accepted:** 03 September 2021

**Published:** 22 September 2021

### Citation:

Li P, Duan J, Cheng Z and Zou H  
(2021) Using Clumped Isotopes to  
Reconstruct the Maximum Burial  
Temperature: A Case Study in the  
Sichuan Basin.  
*Front. Earth Sci.* 9:759372.  
doi: 10.3389/feart.2021.759372

For strata that have experienced continual burial in the early stage and uplift in the late stage, the present-day temperature is lower than the maximum burial temperature (MBT), which is a key parameter for studying the hydrocarbon generation history of source rocks in petroliferous basins. In this paper, a new method for reconstructing the MBT is proposed based on the solid-state reordering model of carbonate clumped isotopes ( $\Delta_{47}$ ). The MBT reconstructed using the  $\Delta_{47}$  was compared with the MBT constrained using the traditional Easy% $R_o$  model. The clumped isotope temperature ( $T_{\Delta_{47}}$ ) of the Permian micritic limestone from the Xibeixiang outcrop (about 62°C) is much higher than its initial formation temperature (20–25°C), suggesting that the limestone experienced partial solid-state reordering during the late burial process. The MBT of the calcite obtained from the solid-state reordering model is 139–147°C, which is quite similar to the MBT determined using the Easy% $R_o$  model (139.5–147.5°C).  $T_{\Delta_{47}}$  of the Permian and Triassic limestone and calcite cements in the Puguang gas field are 150–180°C, while  $T_{\Delta_{47}}$  of the micritic dolostone is about 70°C, suggesting that the  $\Delta_{47}$  of the limestone and calcite cements experienced complete solid-state reordering and the dolostone only experienced partial solid-state reordering. The MBT of the dolomite determined using the solid-state reordering model is 200–220°C, which is also similar to the MBT determined using the Easy % $R_o$  model (202–227°C). Therefore, the case studies from the Sichuan Basin suggest that  $\Delta_{47}$  can be used to reconstruct the MBT of ancient carbonate strata lacking vitrinite and detrital zircon data. However, different types of carbonate samples should be used to reconstruct the MBT for strata that have experienced different temperature histories. Micritic limestone and very finely crystallized dolostone can be used to reconstruct the MBT of strata that have experienced MBTs of <150–200°C and >200–250°C, respectively.

**Keywords:** clumped isotopes, maximum burial temperature, carbonate, solid-state reordering, Sichuan Basin, vitrinite reflectance

## INTRODUCTION

The burial temperature (especially the maximum burial temperature, MBT) of certain strata in a particular sedimentary basin is closely related to the maturity of the organic matter and the hydrocarbon generation of the source rocks (Hunt, 1996; Helgeson et al., 2009; Qiu et al., 2012), and it can also affect the phases in oil and gas reservoirs (Barker, 1990; Hill et al., 2003; Zhu et al., 2018). As a result, the MBT is one of the key parameters for basin modeling and the evaluation of oil and gas resources (Kinley et al., 2008; Qiu et al., 2012; Wood, 2018). For sedimentary basins that have experienced continuous subsidence and burial, the burial depth of certain strata was the largest during the burial process, and its present-day burial temperature is the MBT, which can be determined using current heat flow or geothermal gradient models (Zuo et al., 2011). However, for sedimentary basins that subsided in the early stage and were uplifted and exhumed in the late stage, the present-day burial temperature of certain strata is usually lower than the MBT (Hao et al., 2008; English et al., 2016; Dou et al., 2021), which cannot be directly determined using current heat flow or geothermal gradient models. As a result, reconstructing the MBT of certain strata in a basin that experienced late uplift and exhumation is key to the evaluation of the oil and gas exploration potential, and it is also a research focus in basin modeling.

Common methods of MBT reconstruction include the maturity index of the organic matter (Héroux et al., 1979; Hackley et al., 2015; Luo et al., 2020b) and low temperature thermochronology (Carlson, 1990; Craddock and Houseknecht, 2016; Ehlers and Farley, 2003; Yamada et al., 2007). The maturity index of the organic matter is commonly characterized by the vitrinite reflectance (Mukhopadhyay, 1994; Katz and Lin, 2021), which is mainly controlled by the temperature (Hunt, 1996). Therefore, the current vitrinite reflectance ( $R_o$ ), combined with an organic matter maturation model (such as the Easy% $R_o$  model; Sweeney and Burnham, 1990), can be used to determine the MBT. For strata without vitrinite data, the bitumen reflectance and graptolite reflectance can be used to calculate the equivalent  $R_o$  (Jacob, 1989; Luo et al., 2020b), but different conversion methods exist, and they have different application scopes (Schmidt et al., 2019; Katz and Lin, 2021). Low temperature thermochronology mainly uses annealing kinetic models of fission tracks in minerals (such as apatite and zircon) and (U-Th)/He thermochronology to determine the temperature evolution (Carlson, 1990; Craddock and Houseknecht, 2016; Ehlers and Farley, 2003; Yamada et al., 2007). The annealing kinetic model of apatite fission tracks is only applicable at relatively low temperatures (below 125°C; Carlson, 1990). For strata that have experienced temperatures of >150°C, only the annealing of zircon fission tracks can be used (Yamada et al., 2007), but a unified annealing kinetic model of zircon has not yet been established. The (U-Th)/He thermochronology of zircon can be used to determine the corresponding MBT and time (Reiners, 2005), but for ancient marine strata, detrital zircons are often not easy to obtain, which limits the use of this method. Therefore, for ancient marine strata, both the maturity index of the organic matter and low temperature thermochronology have certain limitations in MBT reconstruction.

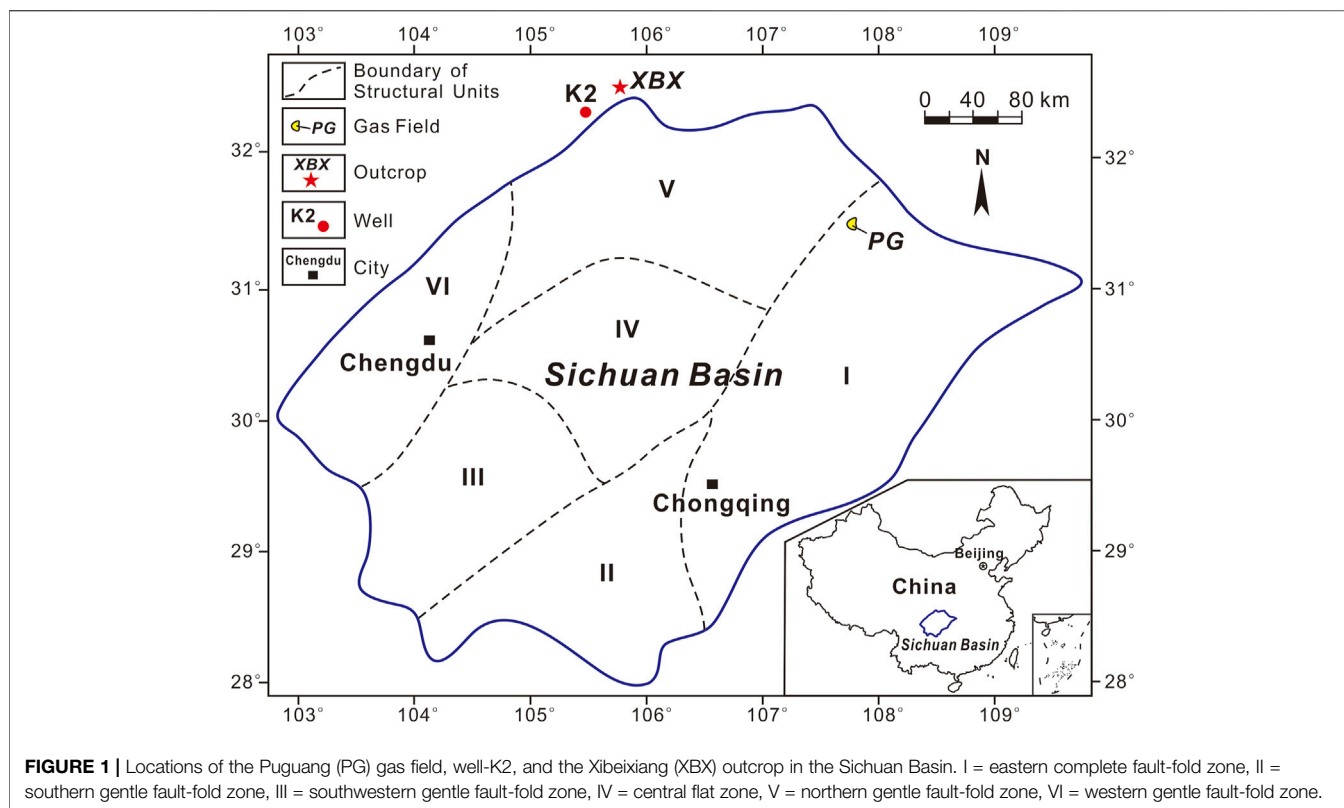
Carbonate minerals (such as calcite and dolomite) are commonly present in ancient marine strata. Carbonate clumped isotopes ( $\Delta_{47}$ ), developed in recent years, can be used to determine the formation temperature of carbonate minerals ( $T_{\Delta 47}$ ), which have been called clumped isotope thermometers (Ghosh et al., 2006; Eiler, 2007). Unlike traditional oxygen isotope ( $\delta^{18}O$ ) thermometers, clumped isotopes can be used to directly determine the formation temperature of carbonate minerals using the abundance of  $^{13}C$ - $^{18}O$  in the carbonate minerals, without relying on the  $\delta^{18}O$  of the fluid from which the carbonate minerals grew (Eiler, 2007). However,  $T_{\Delta 47}$  determined from the clumped isotopes can differ from the original formation temperature due to solid-state reordering. If the carbonate minerals experienced high temperatures during late burial, the  $^{13}C$  and  $^{18}O$  underwent solid-state diffusion, resulting in changes in the abundance of  $^{13}C$ - $^{18}O$  in the minerals and  $T_{\Delta 47}$  of the minerals (Passey and Henkes, 2012; Stolper and Eiler, 2015). Kinetic models of the solid-state reordering of carbonate minerals have been developed in recent years (Passey and Henkes, 2012; Stolper and Eiler, 2015; Lloyd et al., 2018; Hemingway and Henkes, 2021). The carbonate minerals in ancient carbonate strata have usually experienced high temperatures and solid-state reordering of  $^{13}C$  and  $^{18}O$ . Therefore, the solid-state reordering of calcite and dolomite in ancient carbonate strata can be used to reconstruct the MBT according to the established solid-state reordering models for calcite and dolomite (Passey and Henkes, 2012; Stolper and Eiler, 2015; Lloyd et al., 2018). This provides a potential new method for reconstructing the MBT of ancient marine carbonate strata lacking vitrinite and detrital zircon data.

The purpose of this study was to reconstruct the MBT using the clumped isotopes of the Permian and Triassic limestone and dolostone samples from the Sichuan Basin and to compare the MBT determined using carbonate clumped isotopes and the Easy% $R_o$  model in order to verify the reliability of using the carbonate clumped isotope method to reconstruct the MBT and to provide a good case study for MBT reconstruction of ancient marine carbonate strata.

## GEOLOGIC SETTING

The Sichuan Basin is a multi-cycle basin located in southwestern China (Figure 1), with the Ediacaran to Quaternary sediments. It experienced six main tectonic cycles: the Yangtze (before 630 Ma), Caledonian (630–320 Ma), Hercynian (320–252 Ma), Indosinian (252–195 Ma), Yanshanian (195–65 Ma), and Himalayan (65–0 Ma) movements (Zhai, 1989). Among them, the marine deposits were mainly developed from the Yangtze to the Early Indosinian, while the continental deposits were mainly developed from the Late Indosinian to the Himalayan.

The Sichuan Basin experienced early extension and late compression and uplift (Zhai, 1989). From the Yangtze to the Early Indosinian, two weak extension events resulted in the development of two intracratonic sags in the Sichuan Basin (the Early Cambrian Mianyang-Changning sag and the Late Permian Kaijiang-Liangping sag) (Liu et al., 2021). Strong



compression and uplift have occurred since the Late Indosinian, and the Sichuan Basin has evolved into a foreland basin. In particular, the Longmanshan, located in the western boundary of the Sichuan Basin, uplifted gradually from the northeast to the southwest (Burchfiel et al., 1995). During the Yanshanian, many large northeast-southwest striking folds and faults were formed in the eastern Sichuan Basin due to regional northwest-southeast compression (Zhai, 1989). Then, rapid uplift and exhumation occurred during the Late Yanshanian and Himalayan (Deng et al., 2013). It is a typical basin that has experienced early subsidence and late uplift and exhumation in western China.

Marine carbonates and shales were deposited during the Permian and Early Triassic. From the bottom to top, the Permian can be divided into the Liangshan ( $P_{1l}$ ), Qixia ( $P_{1q}$ ), Maokou ( $P_{1m}$ ), Longtan ( $P_{2l}$ )/Wujiaping ( $P_{2w}$ ), and Changxing ( $P_{2c}$ )/Dalong ( $P_{2d}$ ) formations, and the Lower Triassic can be divided into the Feixianguan ( $T_{1f}$ ) and Jialingjiang ( $T_{1j}$ ) formations (Zhai, 1989). The  $P_{2l}/P_{2w}$  and  $P_{2d}$  mainly consist of shales, which are the main source rocks of the  $P_{2c}$  and  $T_{1f}$  gas reservoirs (Li et al., 2005; Yu et al., 2021), while the  $P_{2c}$  and  $T_{1f}$  mainly consist of dolostone and limestone, which are the main reservoir rocks of the main large gas fields (such as the Puguang, Yuanba, and Longgang gas fields) discovered in recent years (Ma et al., 2007; Du et al., 2010; Guo et al., 2018). The dolostone in the  $P_{2c}$  and  $T_{1f}$  was mainly developed on the platform margins of the Kaijiang-liangping trough, and it was formed in a near surface to quite shallow burial environment. The dolomitization fluids were sourced from the  $T_{1f}$  evaporated sea water (Jiang et al., 2014; Li et al., 2021).

## SAMPLING AND ANALYTICAL METHODS

Three  $P_{1q}$  limestone samples (D1, D4, and D6) and two  $P_{2d}$  shale samples were collected from the XBX outcrop (Figure 1), and three  $P_{2c}$ - $T_{1f}$  limestone samples (L56, L61, and L62), four  $P_{2c}$ - $T_{1f}$  dolostone samples (D83, D89, D90, and D99), three  $P_{2c}$ - $T_{1f}$  calcite cement samples (Cem5, Cem8, and Cem25), and thirteen  $P_{2w}$  shale samples were collected from the Puguang (PG) gas field (Figure 1).

All of the shale samples were analyzed for  $R_o$  using conventional microphotometric methods (Stach et al., 1982) at the State Key Laboratory of Petroleum Resources and Prospecting, China University of Petroleum (Beijing). The number of readings was generally >20 for the random reflectance, and the error of each sample was within 0.2%.

Thin sections of all of the limestone and dolostone samples were prepared for petrographic observations. Then, all of the limestone and dolostone samples and calcite cement samples were powdered to less than 0.15 mm (100 mesh) for  $\delta^{13}C$ ,  $\delta^{18}O$ , and clumped isotope ( $\Delta_{47}$ ) analyses at the California Institute of Technology (Caltech). The detailed analytical procedures have been described in previously published papers (Ghosh et al., 2006; Huntington et al., 2009; Ryb and Eiler, 2018; Li et al., 2020). First, about 10 mg of carbonate sample was reacted with 103% phosphoric acid at 90°C, and the  $CO_2$  produced was purified using a gas-chromatography column. Then, the 44–49 masses of the  $CO_2$  were measured using a Thermo MAT253 isotope ratio mass spectrometer. Then, the  $\delta^{13}C$ ,  $\delta^{18}O$ , and  $\Delta_{47}$  values were calculated using the methods described by Huntington et al. (2009). Finally, the  $\Delta_{47}$  values were converted into the absolute reference frame (Dennis et al., 2011), and the

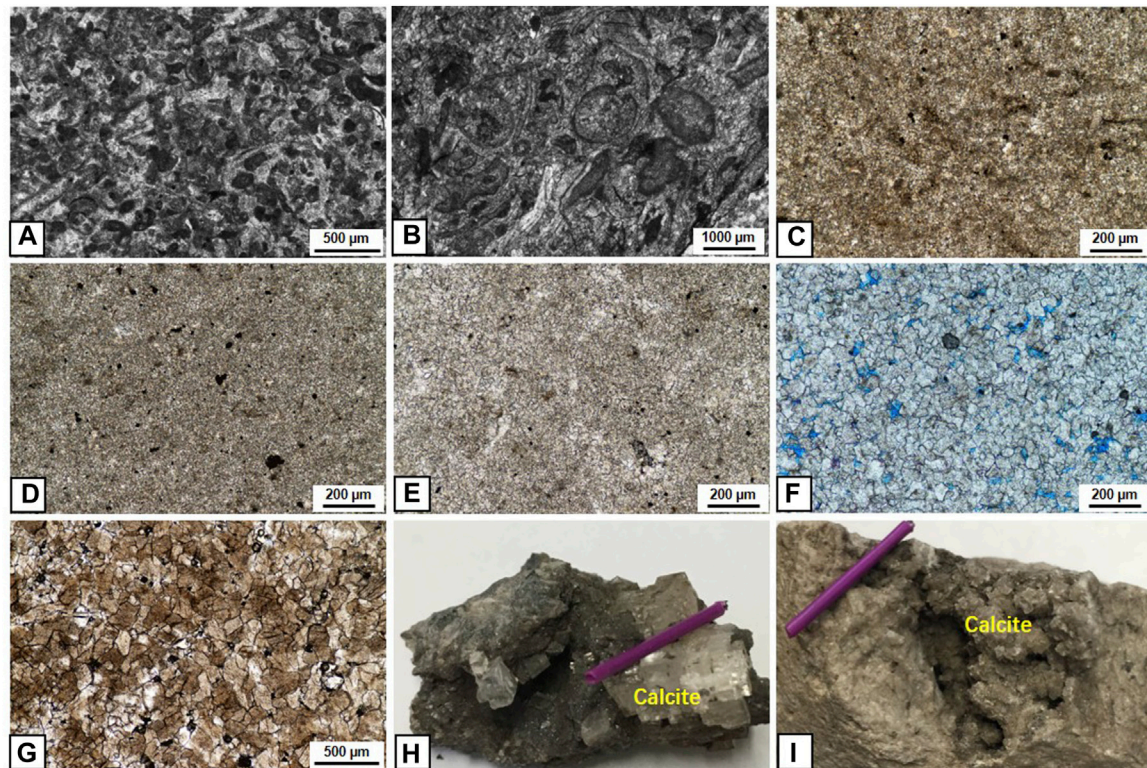


**FIGURE 2 | (A–G)** Thin-section photomicrographs of limestone and dolostone samples, and **(H,I)** photographs of calcite cements. **(A)** Sample D1, XBX outcrop, bioclastic limestone. **(B)** Sample L56, well PG6, 5383.1 m, P<sub>2c</sub>, bioclastic limestone. **(C)** Sample L62, well MB3, 4014.0 m, T<sub>1f</sub>, micritic limestone. **(D)** Sample D83, well MB4, 3892.5 m, T<sub>1f</sub>, micritic dolostone. **(E)** Sample D90, well PG2, 4878.0 m, T<sub>1f</sub>, micritic dolostone. **(F)** Sample D89, well PG12, 6007.0 m, T<sub>1f</sub>, fine crystallized dolostone. **(G)** Sample D99, well PG6, 5339.0 m, P<sub>2c</sub>, medium crystallized dolostone. **(H)** Sample Cem8, well MB3, P<sub>2c</sub>, 4394.6 m, coarse calcite cements (the length of the small purple stick is 2.0 cm). **(I)** Sample Cem5, well DW102, 4825.0 m, T<sub>1f</sub>, coarse calcite cements in vugs in dolostone. Note: the wells MB3, MB4, DW102, PG2, PG6 and PG12 are all located in the Puguang gas field.

clumped isotopes temperature ( $T_{\Delta 47}$ ) of each sample was calculated using the temperature calibrations developed by Bonifacie et al. (2017). Most of the samples were measured two or three times. The standard deviation of the  $\delta^{13}\text{C}$  and  $\delta^{18}\text{O}$  measurement is  $<0.01\%$ , and that of the  $\Delta_{47}$  measurements is  $<0.02\%$ . The standard errors of the in-house standard (CIT Carrara and TV04) were  $<0.01\%$ . The raw data of  $d_{45-d79}$ ,  $D_{47}$  of samples, standards, equilibrated gases and heated gases were listed in the **Supplementary Table 1**.

## RESULTS

### Petrography

The crystal size of the carbonate minerals can be divided into micritic ( $<50\ \mu\text{m}$ ), very fine ( $50\text{--}100\ \mu\text{m}$ ), fine ( $100\text{--}250\ \mu\text{m}$ ), medium ( $250\text{--}500\ \mu\text{m}$ ), and coarse ( $>500\ \mu\text{m}$ ) (Bissell and Chilingar, 1967). All of the limestone samples collected from the XBX outcrop are bioclastic limestone, the cement between the bioclastics is micritic calcite with crystal sizes of  $<10\ \mu\text{m}$ , and no obvious crystallization was observed in the bioclastics and calcite cement (Figure 2A). The limestone samples collected from the Puguang gas field include bioclastic limestone (Figure 2B) and micritic limestone (Figure 2C). The crystal sizes of the calcite are  $<10\ \mu\text{m}$ , and no

obvious crystallization occurred in these limestone samples. The dolostone samples collected from the Puguang gas field include micritic dolostone (Figures 2D,E), very fine crystallized dolostone (Figure 2F), and fine crystallized dolostone (Figure 2G). The crystal size of the two micritic dolostone samples is about  $10\ \mu\text{m}$  (average of  $12\ \mu\text{m}$  for D87 and  $10\ \mu\text{m}$  for D90), and intercrystal pores were hardly observed in the two micritic dolostone samples. The average crystal size of the very fine crystallized dolostone (D89) is about  $70\ \mu\text{m}$ , with very limited dolomite recrystallization, and some pores are developed between the subhedral dolomite crystals (Figure 2F). The crystal sizes of the fine crystallized dolostone (D99) are  $150\text{--}200\ \mu\text{m}$  (average of  $194\ \mu\text{m}$ ), with obvious dolomite recrystallization, and black solid bitumen was observed in the pores between the subhedral dolomite crystals (Figure 2G). The calcite cement samples (crystal sizes of  $0.3\text{--}1.0\ \text{cm}$ ) collected from the Puguang gas field are mainly developed in vugs in dolostone, and it is generally associated with black solid bitumen (Figures 2H,I).

### $\delta^{13}\text{C}$ , $\delta^{18}\text{O}$ , $\Delta_{47}$ , and Clumped Isotope Temperature ( $T_{\Delta 47}$ )

The  $\delta^{13}\text{C}$ ,  $\delta^{18}\text{O}$ ,  $\Delta_{47}$ , and  $T_{\Delta 47}$  values of all of the carbonate samples collected from the XBX outcrop and the Puguang gas field are

**TABLE 1** | The  $\delta^{13}\text{C}$ ,  $\delta^{18}\text{O}$ ,  $\Delta_{47}$ , and  $T_{\Delta 47}$  values of the carbonate samples from the XBX outcrop and the PG gas field in the Sichuan Basin.

Area	Sample ID	Sample Type	Strata	Depth (m)	BT (°C)	N	$\delta^{13}\text{C}$ ‰VPDB	$\delta^{18}\text{O}$ ‰VPDB	$\Delta_{47}$ CDSS0, ‰	$T_{\Delta 47}$ (°C)
XBX	D1*	L	P <sub>2</sub> q	—	17	3	3.878 ± 0.027	-6.336 ± 0.109	0.494 ± 0.008	65.6 ± 3.6
XBX	D4*	L	P <sub>2</sub> q	—	17	3	3.451 ± 0.036	-5.296 ± 0.108	0.514 ± 0.017	56.7 ± 7.0
XBX	D6*	L	P <sub>2</sub> q	—	17	3	3.479 ± 0.008	-4.793 ± 0.038	0.499 ± 0.004	63.3 ± 1.8
PG	Cem5	C	T <sub>1</sub> f	4,825	115	2	-0.840 ± 0.003	-7.732 ± 0.036	0.355 ± 0.008	156.5 ± 7.9
PG	Cem8	C	P <sub>2</sub> c	4,395	108	1	-1.108 ± 0.003	-4.722 ± 0.007	0.368 ± 0.010	145.0 ± 8.9
PG	Cem25	C	P <sub>2</sub> c	4,360	108	2	-0.227 ± 0.004	-6.535 ± 0.005	0.359 ± 0.007	152.7 ± 6.1
PG	L56	L	P <sub>2</sub> c	5,383	133	1	2.505 ± 0.010	-6.943 ± 0.007	0.333 ± 0.013	178.4 ± 14.9
PG	L61	L	T <sub>1</sub> f	5,350	133	1	4.014 ± 0.006	-6.868 ± 0.004	0.347 ± 0.015	163.9 ± 15.6
PG	L62	L	T <sub>1</sub> f	4,014	101	1	3.701 ± 0.004	-6.366 ± 0.005	0.333 ± 0.014	179.1 ± 16.2
PG	D83	MD	T <sub>1</sub> f	3,892	100	3	2.478 ± 0.007	-4.257 ± 0.010	0.479 ± 0.009	72.5 ± 4.5
PG	D90	MD	T <sub>1</sub> f	4,878	123	2	2.748 ± 0.001	-4.044 ± 0.005	0.481 ± 0.019	71.7 ± 8.9
PG	D89	VFCD	T <sub>1</sub> f	6,007	137	2	2.765 ± 0.005	-4.209 ± 0.005	0.449 ± 0.009	88.5 ± 5.4
PG	D99	FCD	P <sub>2</sub> c	5,339	128	2	3.903 ± 0.005	-6.300 ± 0.008	0.391 ± 0.010	126.3 ± 7.6

Note: L = limestone, C = calcite, MD = micritic dolostone, VFCD = very fine crystallized dolostone, FCD = fine crystallized dolostone, BT = burial temperature. N is the number of sample tests, the  $\delta^{13}\text{C}$ ,  $\delta^{18}\text{O}$ , and  $\Delta_{47}$  values are the average values of each measurement, the errors of the  $\delta^{13}\text{C}$ ,  $\delta^{18}\text{O}$ , and  $\Delta_{47}$  values are average standard deviations.  $T_{\Delta 47}$  was calculated using the following equation:  $\Delta_{47} \text{ CDSS0} = 0.0422 \times 10^6 \times T^{-2} + 0.1262$  (Bonifacie et al., 2017). \* denotes from Li et al. (2020).

**TABLE 2** | The vitrinite reflectance ( $R_o$ ) of the shale samples from the XBX outcrop and PG gas field in the Sichuan Basin.

Area	Well	Depth (m)	Strata	Number of measuring points	$R_o$ (%)
XBX	—	—	P <sub>2</sub> d	20	0.92
XBX	—	—	P <sub>2</sub> d	20	0.96
PG	MB3	4,891–4,892	P <sub>2</sub> w	34	2.39
PG	MB3	4,930–4,933	P <sub>2</sub> w	27	2.43
PG	MB3	4,952–4,954	P <sub>2</sub> w	33	2.67
PG	MB3	4,952–4,954	P <sub>2</sub> w	25	2.60
PG	MB3	5,153–5,157	P <sub>2</sub> w	34	2.71
PG	MB3	5,185–5,186	P <sub>2</sub> w	20	2.79
PG	MB3	5,185–5,186	P <sub>2</sub> w	21	2.76
PG	PG5	5,586–5,591	P <sub>2</sub> w	25	3.05
PG	PG5	5,596–5,602	P <sub>2</sub> w	25	2.95
PG	PG5	5,674–5,678	P <sub>2</sub> w	25	3.19
PG	PG5	5,681–5,687	P <sub>2</sub> w	30	2.68
PG	PG5	5,732–5,734	P <sub>2</sub> w	24	3.10
PG	PG5	5,744–5,747	P <sub>2</sub> w	36	3.11

presented in **Table 1**. The  $\delta^{13}\text{C}$ ,  $\delta^{18}\text{O}$ , and  $\Delta_{47}$  values of the three limestone samples from the XBX outcrop range from 3.451 to 3.788‰, -6.336‰ to -4.793‰, and 0.499–0.514‰. For the limestone, dolostone, and calcite cement samples collected from then Puguang gas field, the  $\delta^{13}\text{C}$  values range from 2.505 to 4.014‰, 2.478–3.903‰, and -1.108‰ to -0.227‰, respectively; the  $\delta^{18}\text{O}$  values range from -6.943‰ to -6.366‰, -6.300‰ to -4.044‰, and -7.732‰ to -4.722‰, respectively; and the  $\Delta_{47}$  values range from 0.333 to 0.347‰, 0.391–0.481‰, and 0.355–0.368‰, respectively. The  $\delta^{13}\text{C}$  values of the limestone and dolostone samples from the Puguang gas field are basically similar (2.505–4.014‰), while the  $\delta^{13}\text{C}$  values of the calcite cement (-1.108‰ to -0.227‰) are significantly lower than those of the limestone and dolostone samples.

$T_{\Delta 47}$  of all of the carbonate samples exhibit a relatively large variation (**Table 1**).  $T_{\Delta 47}$  of the limestone from the XBX outcrop are 57.6–65.6°C (average of 61.9°C); while  $T_{\Delta 47}$  of the calcite cement and limestone samples from the Puguang gas field are

145–156.5°C (average of 151.4°C) and 163.9–179.1°C (average of 173.8°C), respectively. There is a large difference in  $T_{\Delta 47}$  of the four dolostone samples from the Puguang gas field.  $T_{\Delta 47}$  of the two micritic dolostone samples are  $71.7 \pm 8.9^\circ\text{C}$  (D90) and  $72.5 \pm 4.5^\circ\text{C}$  (D83), that of the very fine crystallized dolostone is  $88.5 \pm 5.4^\circ\text{C}$ , and that of the fine crystallized dolostone is  $126.3 \pm 7.6^\circ\text{C}$  (D99).

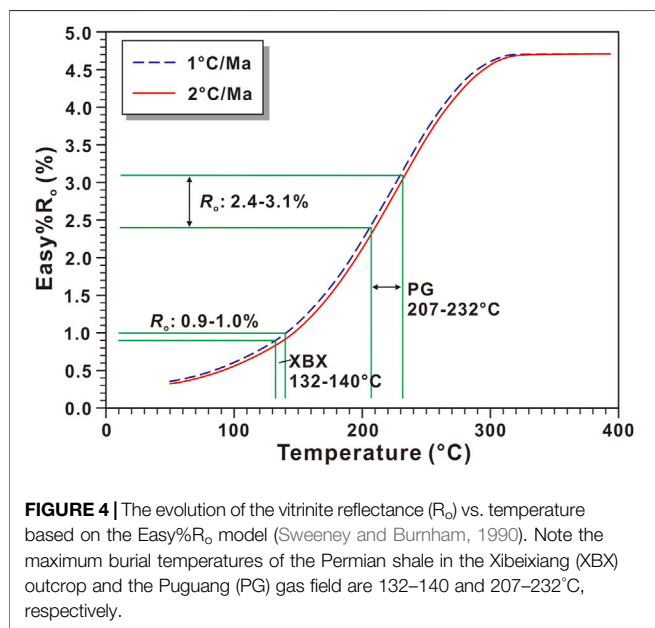
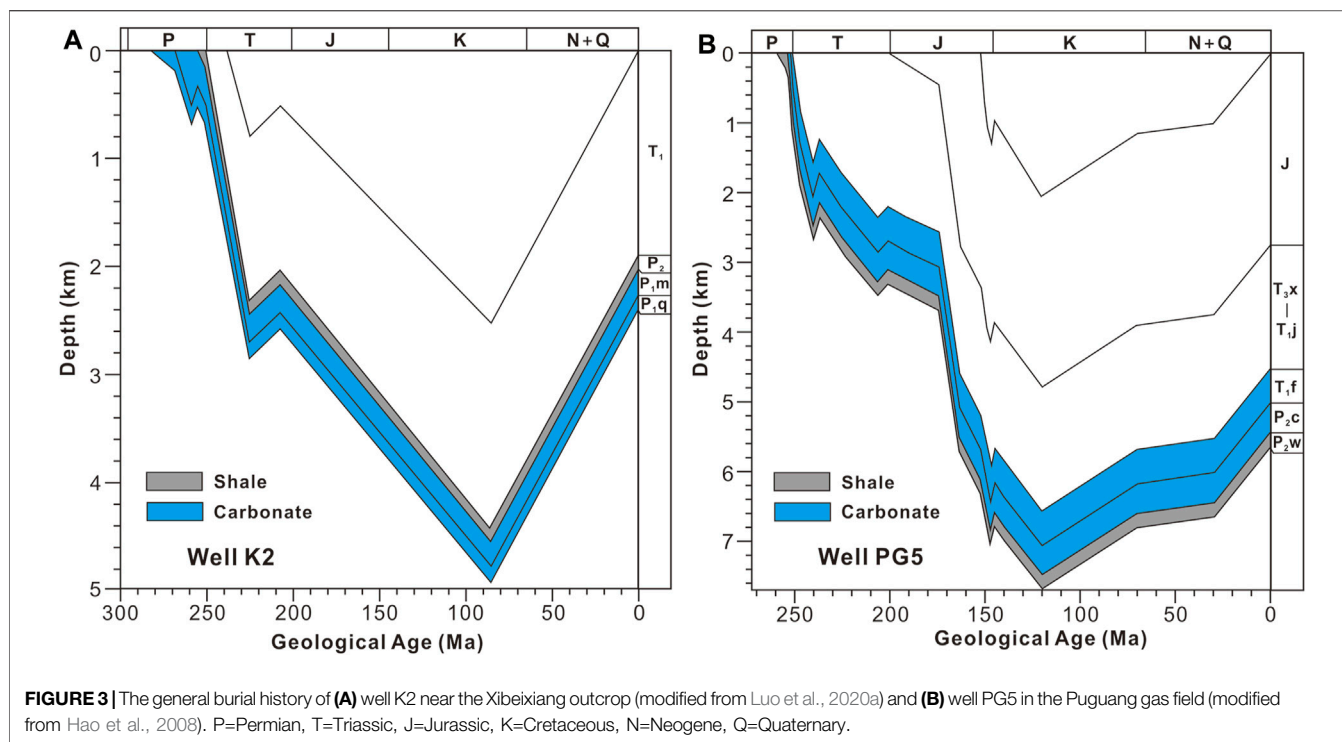
## Vitrinite Reflectance ( $R_o$ )

The  $R_o$  values of the Permian shales from the XBX outcrop and the Puguang gas field are presented in **Table 2**. The  $R_o$  values of the two P<sub>2</sub>d shale samples from the XBX outcrop are 0.92 and 0.96%, while the  $R_o$  values of the P<sub>2</sub>w shales from the Puguang gas field are 2.39–3.11% (average of 2.80%).

## DISCUSSION

### EASY% $R_o$ Model and Maximum Burial Temperature Reconstruction for the Xibeixiang Outcrop and Puguang Gas Field

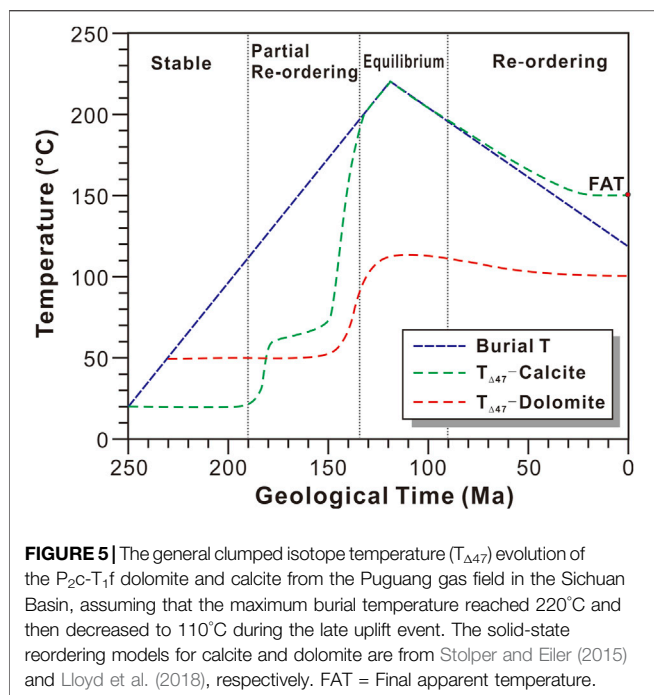
The maturity of organic matter, which is usually characterized by  $R_o$  and/or equivalent  $R_o$  (such as the solid bitumen reflectance or graptolite reflectance), is a commonly used method for paleotemperature reconstruction (Mukhopadhyay, 1994; Hackley et al., 2015; Luo et al., 2020b). The maturity evolution of organic matter is an irreversible process and can be characterized by a first-order chemical kinetics reaction. According to the Arrhenius equation, the maturity of organic matter has an exponential relationship with temperature and a linear relationship with time. As a result, temperature is the most important parameter affecting the maturity evolution of organic matter (Hunt, 1996). Theoretically, the MBT can be obtained based on a model of the evolution of the organic matter's maturity with temperature (such as the EASY% $R_o$  model; Sweeney and Burnham, 1990).



The EASY% $R_o$  model is a widely accepted model for the evolution of the maturity of organic matter, and the organic matter maturity ( $R_o$ ) can be calculated for a given heating rate (Sweeney and Burnham, 1990). According to apatite fission track analysis (Deng et al., 2013), the Permian and Triassic strata in the XBX outcrop and the Puguang gas field reached their maximum burial depths at about 80 and 120 Ma, respectively (Figure 3). The area of the XBX outcrop was uplifted in the Late Indosinian

(Burchfiel et al., 1995), and the  $R_o$  of the Permian shale near the XBX outcrop in the NW Sichuan Basin is <1.3% (Fu et al., 2010), so the MBT of the Permian shale should be less than 160°C (Figure 4). A lot of solid bitumen with a relatively high maturity ( $R_o > 1.7\%$ ) is commonly present in the Permian and Triassic gas reservoir in the Puguang gas field, suggesting that large scale oil-cracking occurred in this gas field, and the maximum burial temperature may have exceeded 200°C (Hao et al., 2008). In addition, the heat flow has decreased gradually since the Late Permian (Zhu et al., 2016). Thus, the burial temperature of the Permian and Triassic strata in the XBX outcrop and the Puguang gas field should have reached the maximum values when the burial depths reached the maximum values at about 80 and 120 Ma (Figure 3). As a result, the heating rates should be about 1.0°C/Ma ( $150^\circ\text{C}/(260-80 \text{ Ma}) = 0.83^\circ\text{C}/\text{Ma}$ ) and 2.0°C/Ma ( $220^\circ\text{C}/(250-120 \text{ Ma}) = 1.7^\circ\text{C}/\text{Ma}$ ) for the XBX outcrop and the Puguang gas field, respectively.

The evolution of  $R_o$  with temperature based on the EASY% $R_o$  model for heating rates of 1.0 and 2.0°C/Ma is shown in Figure 4. According to this model,  $R_o$  of the  $P_2d$  shale in the XBX outcrop is 0.92–0.96%, so the MBT of the  $P_2d$  should be 132–140°C, while  $R_o$  of the  $P_2w$  shale in the Puguang gas field is 2.39–3.11%, so the MBT of the  $P_2w$  should be 207–232°C (Figure 4). The thicknesses of the intervals between the  $P_{1q}$  limestone and the  $P_2d$  shale in the XBX outcrop and between the  $P_{2c}$ - $T_{1f}$  dolostone and the  $P_2w$  shale in the Puguang gas field are about 300 and 200 m (Figure 3), respectively. In addition, the paleotemperature gradient in the Late Cretaceous was about 25°C/km (Zhu et al., 2016). As a result, the MBTs of the  $P_{1q}$  limestone in the XBX outcrop and the  $P_{2c}$ - $T_{1f}$  dolostone in the Puguang gas field should be 139.5–147.5 and 202–227°C, respectively. The MBT determined using the



EASY% $R_o$  model supplies a basic constraint on the MBT determined using the solid-state reordering model of carbonate clumped isotopes.

### Solid-State Reordering of Calcite and Maximum Burial Temperature of $P_1q$ in the Xibeixiang Outcrop

Carbonate clumped isotopes ( $\Delta_{47}$ ) can be used to directly determine the formation temperature or the equilibrium temperature of carbonate minerals, and they are independent of the  $\delta^{18}O$  of the fluid from which the carbonate minerals were deposited. This is called the clumped isotope thermometer (Ghosh et al., 2006; Eiler, 2007). The clumped isotope thermometer is mainly based on the exchange reactions of the  $^{13}C$  and  $^{18}O$  in carbonate minerals, and the abundance of  $^{13}C$ - $^{18}O$  in carbonate minerals is a function of temperature (Eiler, 2007). However, the clumped isotope temperature ( $T_{\Delta 47}$ ) may be altered by high temperatures and/or recrystallization during the late burial process and can be completely different from the original formation temperature (Passey and Henkes, 2012). Ancient carbonate minerals have usually experienced relatively high temperatures during late burial, which resulted in solid-state exchange (reordering) of the  $^{13}C$ - $^{18}O$  in the carbonate minerals. Consequently, the abundances of  $^{13}C$ - $^{18}O$  in carbonate minerals will differ from the original abundances when the carbonate minerals were formed, and the  $T_{\Delta 47}$  values should also be different from the original formation temperature of the carbonate minerals. In addition, recrystallization after mineral formation can also change the abundance of  $^{13}C$ - $^{18}O$  and  $T_{\Delta 47}$  of the carbonate minerals (Ryb and Eiler, 2018). Therefore, for ancient carbonate minerals, the

present-day  $T_{\Delta 47}$  is often the result of the combined effect of recrystallization and solid-state reordering. The solid-state reordering of  $\Delta_{47}$  can be characterized using a kinetic model, and the MBT of the carbonate minerals can be reconstructed if the carbonate minerals experienced no or limited recrystallization.

There are two main kinetic models for characterizing the solid-state reordering of carbonate minerals: the transient defect/equilibrium defect model (Henkes et al., 2014) and the exchange-diffusion model (Stolper and Eiler, 2015). The best agreement between model predictions and natural dolomite marbles was found when using the exchange-diffusion model (Lloyd et al., 2018). Therefore, the exchange-diffusion model was used in this study. According to the exchange-diffusion model, the variation of  $T_{\Delta 47}$  was shown in Figure 5, if the Permian-Triassic limestone was formed at about 30°C and reached a maximum temperature of about 220°C at 120 Ma. When the burial temperature was <100°C, no solid-state reordering occurred and  $T_{\Delta 47}$  of the calcite would be stable. When the burial temperature was between 100 and 200°C, partial solid-state reordering occurred and  $T_{\Delta 47}$  of the calcite increased as the burial temperature increased. When the burial temperature was >200°C, full solid-state reordering occurred and  $T_{\Delta 47}$  of the calcite reached equilibrium with the burial temperature. When the burial temperature was <200°C during the late uplift and exhumation, partial solid-state reordering occurred again and  $T_{\Delta 47}$  of the calcite decreased as the burial temperature decreased. If the burial temperature was decreased from above 200°C to below 150°C during the uplift,  $T_{\Delta 47}$  of the calcite would have decreased to a blocking temperature (final apparent temperature) of about 175–200°C (Henkes et al., 2014), and it did not decrease as the burial temperature decreased (Figure 5). The solid-state reordering of dolomite is similar to that of calcite, but  $T_{\Delta 47}$  of dolomite is stable when the burial temperature is <150°C, and it does not reach equilibrium with the burial temperature when the burial temperature is <250–300°C (Lloyd et al., 2018).

$T_{\Delta 47}$  of the limestone from the XBx outcrop is 62°C on average, which is significantly higher than the seawater temperature (20–30°C) during the deposition of  $P_1q$  (Henkes et al., 2018), but is far lower than the blocking temperature after reaching the equilibrium temperature. According to the kinetic model of the solid-state reordering of calcite, it can be inferred that the limestone only underwent partial solid-state reordering, and it did not reach equilibrium. The petrological characteristics of the three bioclastic limestone samples (D1–D3) from the XBx outcrop show that the bioclastics were cemented with micritic calcite, and no obvious recrystallization was observed. Therefore, the  $T_{\Delta 47}$  values of the present-day limestone samples were mainly affected by the solid-state reordering process. As a result, the solid-state reordering model can be used to reconstruct the MBT of these limestone samples. Based on the solid-state reordering model for the calcite in the XBx outcrop, the relationship between  $T_{\Delta 47}$  and MBT is shown in Figure 6.  $T_{\Delta 47}$  of the present-day limestone is 62°C, and the corresponding MBT of the XBx limestone is about 139–147°C (Figure 6), which is basically consistent with the MBT constrained by the EASY%  $R_o$  model (139.5–147.5°C).

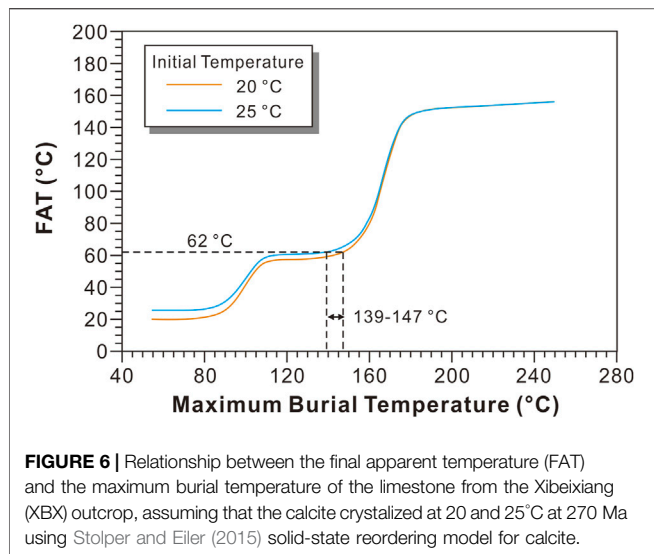


**FIGURE 6** | Relationship between the final apparent temperature (FAT) and the maximum burial temperature of the limestone from the Xibeixiang (XBX) outcrop, assuming that the calcite crystallized at 20 and 25°C at 270 Ma using Stolper and Eiler (2015) solid-state reordering model for calcite.

## Solid-State Reordering of Dolomite and the Maximum Burial Temperature of the P<sub>2</sub>c-T<sub>1</sub>f in the Puguang Gas Field

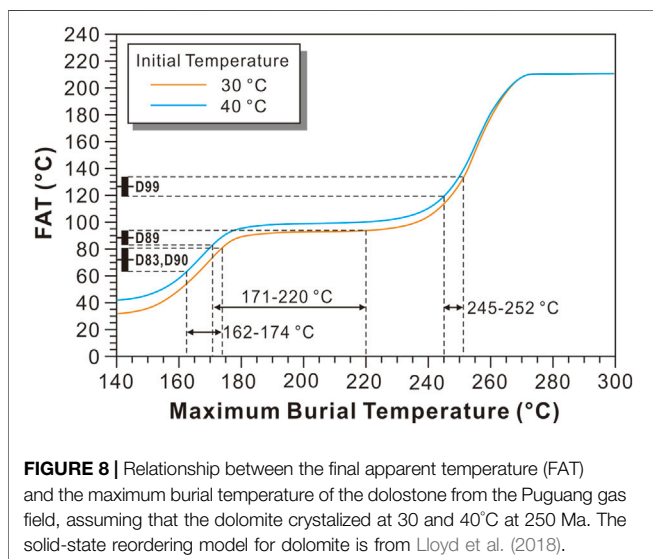
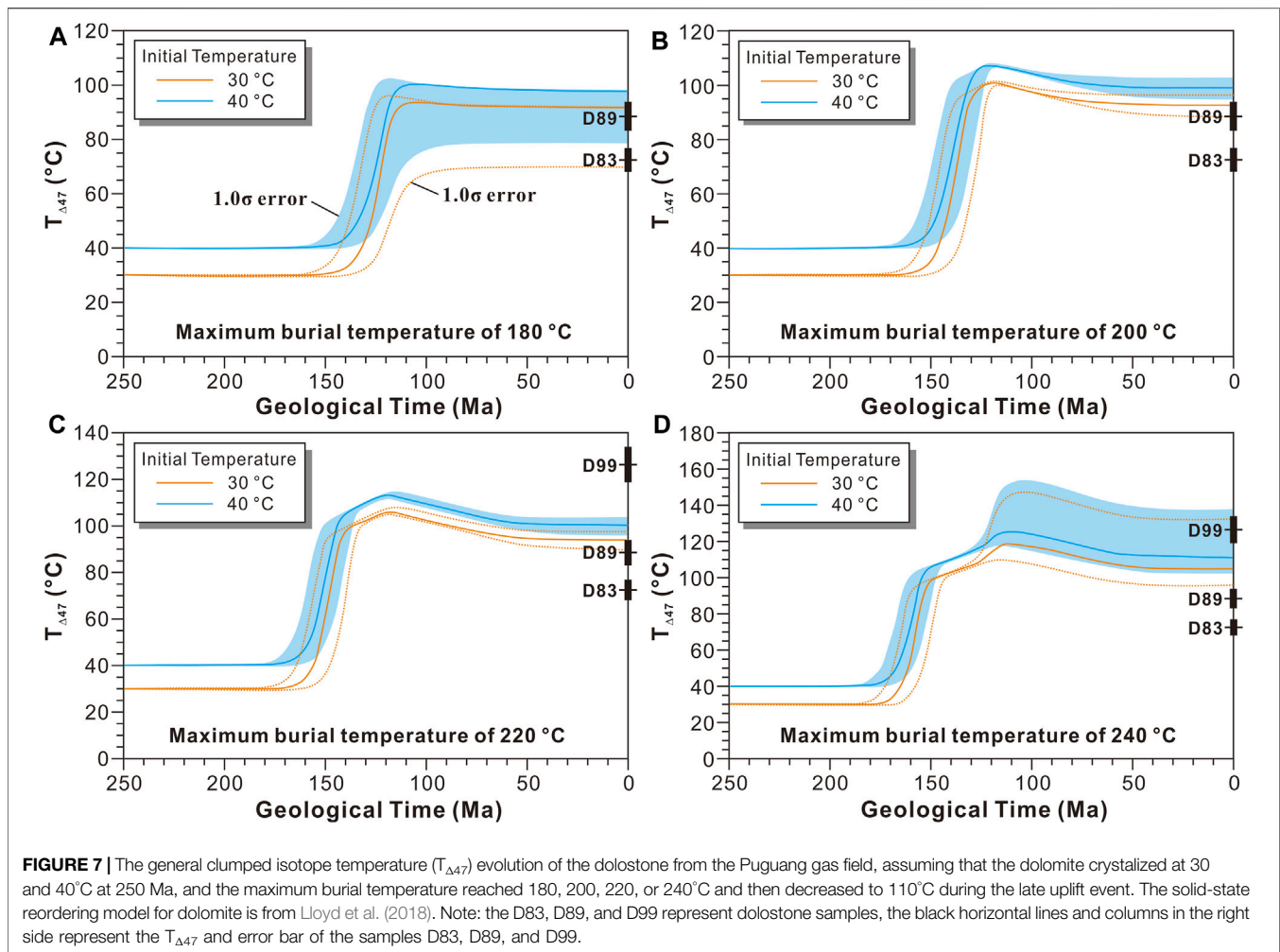
The MBT determined using the EASY%R<sub>0</sub> model is >200°C (202–227°C; **Figure 4**), which supports the fact that widespread oil cracking occurred in the Puguang gas field (Hao et al., 2008), while the present-day burial temperature of the P<sub>2</sub>c-T<sub>1</sub>f is 100–135°C. According to the solid-state reordering model of calcite (**Figure 5**) and the temperature history of the Puguang gas field, the limestone or early-formed calcite cements should have experienced complete solid-state reordering, and the final apparent temperature of the limestone and calcite cement should be similar to the blocking temperature (150–160°C) because the present-day burial temperature is 100–135°C due to the late uplift and exhumation. T<sub>Δ47</sub> of the micritic limestone and bioclastic limestone is 150–170°C, which is consistent with the blocking temperature predicted by the solid-state reordering model for calcite. The coarse calcite cements, associated with the solid bitumen and having more negative δ<sup>13</sup>C values (–1.108‰ to –0.227‰) than that of its bulk rock (dolostone), are considered to be the product of oil cracking and thermochemical sulfate reduction (TSR) processes (Hao et al., 2008), and they were deposited during the early burial process not during the late uplift and exhumation. T<sub>Δ47</sub> of the calcite cements in the Puguang gas field are 145–156.5°C (average of 151.4°C), which is also very close to the blocking temperature of calcite predicted by the model. The small differences in the final apparent temperatures of the limestone and the coarse calcite cements in the Puguang gas field according to the uniform solid-state reordering model may be due to the different kinetic parameters used in the solid-state reordering models of the coarse calcite and micritic limestone, especially during the cooling process. However, no published paper has discussed this problem, and it is not discussed in detail in this paper. However, it is certain that the relatively high temperature (>200°C) in the Puguang gas field resulted in the complete solid-state reordering of the micritic limestone and the

coarse calcite cements. Therefore, the micritic limestone and coarse calcite cements cannot be used to reconstruct the MBT in the Puguang gas field.

However, the temperature of the onset of the partial reordering of dolomite is much higher than that of calcite, and the complete solid-state reordering temperature of dolomite can be as high as 250–300°C (Lloyd et al., 2018). As a result, the solid-state reordering of the dolostone samples can be used to reconstruct the MBT in the Puguang gas field. The T<sub>Δ47</sub> values of the dolostone with different dolomite crystal sizes from the Puguang gas field are significantly different (**Table 1**). T<sub>Δ47</sub> of the micritic dolostone (71.7–72.5°C) is the lowest, followed by T<sub>Δ47</sub> of the very finely crystallized dolostone (88.5 ± 5.4°C), but T<sub>Δ47</sub> of the two types of dolostone are very close to each other. T<sub>Δ47</sub> of the finely crystallized dolostone (126.3 ± 7.6°C) is significantly higher than that of the micritic dolostone and the very finely crystallized dolostone, suggesting that T<sub>Δ47</sub> of the finely crystallized dolostone was also affected by relatively strong recrystallization, while the very finely crystallized dolostone only experienced very limited recrystallization.

It is widely accepted that the micritic and very finely crystallized dolostones were caused by penecontemporaneous dolomitization, which occurred under near surface conditions or quite shallow burial conditions. As a result, the initial formation temperatures of the micritic and very finely crystallized dolostones should be similar to the temperature of the coeval seawater. The temperature (30–40°C) in Southern China was lethally hot during the Late Permian–Early Triassic (Sun et al., 2012), so the initial formation temperature of the micritic and very finely crystallized dolostones can be assumed to be 30–40°C. Assuming that the MBT reached 180°C, 200°C, 220°C, and 240°C, the corresponding T<sub>Δ47</sub> evolution of the dolostone can be predicted using the solid-state reordering model for dolomite (**Figure 7**). If the MBT reached 180°C, only T<sub>Δ47</sub> of the micritic dolostone (D83) and the very finely crystallized dolostone (D89) are within the predicted range (1.0 σ error included; **Figure 7A**), while T<sub>Δ47</sub> of the finely crystallized dolostone (D99) is significantly higher than the predicted range. If the MBT reached 200°C or 220°C, only T<sub>Δ47</sub> of the very finely crystallized dolostone (D89) is within the predicted range, and T<sub>Δ47</sub> of the micritic dolostone and the finely crystallized dolostone (D99) are slightly lower and significantly higher than the predicted range, respectively (**Figures 7B,C**). If the MBT reached 240°C, only T<sub>Δ47</sub> of the finely crystallized dolostone (D99) is within the predicted range, and T<sub>Δ47</sub> of the micritic dolostone and the very finely crystallized dolostone are lower than the predicted range (**Figure 7D**). As was discussed above, T<sub>Δ47</sub> of the limestone and calcite cements were similar to the blocking temperature during the late cooling process, suggesting that the calcite experienced complete solid-state reordering, and the MBT should be >200°C. Combined with the T<sub>Δ47</sub> evolution shown in **Figure 6**, the MBT of the P<sub>2</sub>c-T<sub>1</sub>f in the PG gas field should be 200–220°C, which is similar to the MBT determined using the EASY%R<sub>0</sub> model (202–227°C).

Based on the model of the relationship between the final apparent temperature (present-day T<sub>Δ47</sub>) and the MBT (**Figure 8**), the MBTs determined using the present-day T<sub>Δ47</sub> of the micritic dolostone (D83 and D90), the very finely crystallized dolostone (D89), and the finely



crystallized dolomite (D99) are 162–174, 171–220, and 245–252 °C, respectively. Only the MBT determined using the finely crystallized dolomite falls within the temperature range determined using the

EASY% $R_0$  model. The MBT determined using the micritic dolomite is slightly lower than the temperature range determined using the EASY% $R_0$  model. This may be due to the kinetic parameter of the solid-state reordering model for dolomite was constructed based on dolomite with some recrystallization. While the MBT determined using the finely crystallized dolomite is significantly higher than the temperature range determined using the EASY% $R_0$  model, which is most likely due to the occurrence of significant recrystallization. However, the time and temperature at which the recrystallization reached final equilibrium is unknown. Consequently, the present-day  $T_{\Delta 47}$  of the finely crystallized dolomite cannot be used to determine the MBT. Perhaps U-Pb dating of carbonate can be used to accurately determine the final equilibrium age of the dolomite (Pan et al., 2020), and combined with the general burial and thermal gradient information, it can be used to reconstruct the MBT based on the solid-state reordering model, which is a valuable research direction for future studies.

## CONCLUSION

The maximum burial temperature (MBT) of the XBX outcrop and the Puguang gas field was reconstructed using the solid-state

reordering models for calcite and dolomite. The MBTs of the P<sub>1</sub>q limestone in the XBX outcrop and the P<sub>2</sub>c-T<sub>1</sub>f dolostone in the Puguang gas field determined using the solid-state reordering models for calcite and dolomite are 139–147 and 200–220°C, respectively, which are similar to the ranges determined using the EASY%R<sub>0</sub> model (139.5–147.5 and 202–227°C, respectively). Based on this study in the Sichuan Basin, the solid-state reordering models for calcite and dolomite provide a new potential method for reconstructing the MBT of ancient carbonate strata with MBTs of <150–200 and 250–300°C, respectively. In particular, the MBT determined using the solid-state reordering model for dolostone with limited crystallization is acceptable, while that of dolostone with obvious crystallization is significantly higher than the actual MBT. In addition, the solid-state reordering kinetic model for micritic dolostone also needs to be further optimized in future research.

## DATA AVAILABILITY STATEMENT

The original contributions presented in the study are included in the article/**Supplementary Materials**, further inquiries can be directed to the corresponding author.

## REFERENCES

- Barker, C. (1990). Calculated Volume and Pressure Changes during the thermal Cracking of Oil to Gas in Reservoirs. *AAPG Bull.* 74, 1254–1261. doi:10.1306/0c9b247f-1710-11d7-8645000102c1865d
- Bissell, H. J., and Chilingar, G. V. (1967). "Chapter 4 Classification of Sedimentary Carbonate Rocks," in *Carbonate rocks: Origin, occurrence and classification—Development in sedimentology* 9A. Editors G. V. Chilingar, H. J. Bissell, and R. W. Fairbridge (Amsterdam: Elsevier), 87–168. doi:10.1016/s0070-4571(08)71112-9
- Bonifacie, M., Calmels, D., Eiler, J. M., Horita, J., Chaduteau, C., Vasconcelos, C., et al. (2017). Calibration of the Dolomite Clumped Isotope Thermometer from 25 to 350 °C, and Implications for a Universal Calibration for All (Ca, Mg, Fe) CO<sub>3</sub> Carbonates. *Geochimica et Cosmochimica Acta* 200, 255–279. doi:10.1016/j.gca.2016.11.028
- Burchfiel, B. C., Zhiliang, C., Yupinc, L., and Royden, L. H. (1995). Tectonics of the Longmen Shan and Adjacent Regions, central China. *Int. Geology. Rev.* 37, 661–735. doi:10.1080/00206819509465424
- Carlson, W. D. (1990). Mechanisms and Kinetics of Apatite Fission-Track Annealing. *Am. Mineral.* 75, 1120–1139.
- Craddock, W. H., and Houseknecht, D. W. (2016). Cretaceous–Cenozoic Burial and Exhumation History of the Chukchi Shelf, Offshore Arctic Alaska. *Bulletin* 100, 63–100. doi:10.1306/09291515010
- Deng, B., Liu, S.-g., Li, Z.-w., Jansa, L. F., Liu, S., Wang, G.-z., et al. (2013). Differential Exhumation at Eastern Margin of the Tibetan Plateau, from Apatite Fission-Track Thermochronology. *Tectonophysics* 591, 98–115. doi:10.1016/j.tecto.2012.11.012
- Dennis, K. J., Affek, H. P., Passey, B. H., Schrag, D. P., and Eiler, J. M. (2011). Defining an Absolute Reference Frame for 'clumped' Isotope Studies of CO<sub>2</sub>. *Geochimica et Cosmochimica Acta* 75, 7117–7131. doi:10.1016/j.gca.2011.09.025
- Dou, L., Wang, R., Wang, J., Cheng, D., Green, P. F., and Wei, X. (2021). Thermal History Reconstruction from Apatite Fission-Track Analysis and Vitrinite Reflectance Data of the Bongor Basin, the Republic of Chad. *Bulletin* 105, 919–944. doi:10.1306/11182019167

## AUTHOR CONTRIBUTIONS

PL, Conceptualization, Methodology, Writing-Original Draft; JD, Resources; ZC, Investigation; HZ, Supervision, Funding acquisition.

## FUNDING

This study was supported by the Strategic Priority Research Program of the Chinese Academy of Sciences (No. XDA14010306), NSFC Basic Research Program on Deep Petroleum Resource Accumulation and Key Engineering Technologies (U19B6003).

## ACKNOWLEDGMENTS

We thank Uri Ryb and Nami Kitchen at Caltech for clumped isotopes measurement.

## SUPPLEMENTARY MATERIAL

The Supplementary Material for this article can be found online at: <https://www.frontiersin.org/articles/10.3389/feart.2021.759372/full#supplementary-material>

- Du, J. H., Xu, C. C., Wang, Z. C., Shen, P., He, H. Q., Yang, Y., et al. (2010). *Natural gas exploration of Permian-Triassic reef & oolite in Sichuan Basin*. Beijing: Petroleum Industry Press, 1–160. (in Chinese).
- Ehlers, T. A., and Farley, K. A. (2003). Apatite (U-Th)/He Thermochronometry: Methods and Applications to Problems in Tectonic and Surface Processes. *Earth Planet. Sci. Lett.* 206, 1–14. doi:10.1016/s0012-821x(02)01069-5
- Eiler, J. M. (2007). "Clumped-isotope" Geochemistry-The Study of Naturally-Occurring, Multiply-Substituted Isotopologues. *Earth Planet. Sci. Lett.* 262, 309–327. doi:10.1016/j.epsl.2007.08.020
- English, K. L., Redfern, J., Corcoran, D. V., English, J. M., and Cherif, R. Y. (2016). Constraining Burial History and Petroleum Charge in Exhumed Basins: New Insights from the Illizi Basin, Algeria. *Bulletin* 100, 623–655. doi:10.1306/12171515067
- Fu, X. D., Qin, J. Z., Tenger, and Wang, X. F. (2010). Evaluation on Dalong Formation Source Rock in the north Sichuan Basin. *Pet. Geology. Exp.* 32, 566–571. (in Chinese with English abstract).
- Ghosh, P., Adkins, J., Affek, H., Balta, B., Guo, W., Schauble, E. A., et al. (2006). 13C-18O Bonds in Carbonate Minerals: A New Kind of Paleothermometer. *Geochimica et Cosmochimica Acta* 70, 1439–1456. doi:10.1016/j.gca.2005.11.014
- Guo, X., Hu, D., Li, Y., Duan, J., Ji, C., and Duan, H. (2018). Discovery and Theoretical and Technical Innovations of Yuanba Gas Field in Sichuan Basin, SW China. *Pet. Exploration Dev.* 45, 15–28. doi:10.1016/s1876-3804(18)30002-8
- Hackley, P. C., Araujo, C. V., Borrego, A. G., Bouzinos, A., Cardott, B. J., Cook, A. C., et al. (2015). Standardization of Reflectance Measurements in Dispersed Organic Matter: Results of an Exercise to Improve Interlaboratory Agreement. *Mar. Pet. Geology* 59, 22–34. doi:10.1016/j.marpetgeo.2014.07.015
- Hao, F., Guo, T., Zhu, Y., Cai, X., Zou, H., and Li, P. (2008). Evidence for Multiple Stages of Oil Cracking and Thermochemical Sulfate Reduction in the Puguang Gas Field, Sichuan Basin, China. *Bulletin* 92, 611–637. doi:10.1306/01210807090
- Helgeson, H. C., Richard, L., McKenzie, W. F., Norton, D. L., and Schmitt, A. (2009). A Chemical and Thermodynamic Model of Oil Generation in Hydrocarbon Source Rocks. *Geochimica et Cosmochimica Acta* 73, 594–695. doi:10.1016/j.gca.2008.03.004

- Hemingway, J. D., and Henkes, G. A. (2021). A Disordered Kinetic Model for Clumped Isotope Bond Reordering in Carbonates. *Earth Planet. Sci. Lett.* 566, 116962. doi:10.1016/j.epsl.2021.116962
- Henkes, G. A., Passey, B. H., Grossman, E. L., Shenton, B. J., Pérez-Huerta, A., and Yancey, T. E. (2014). Temperature Limits for Preservation of Primary Calcite Clumped Isotope Paleotemperatures. *Geochimica et Cosmochimica Acta* 139, 362–382. doi:10.1016/j.gca.2014.04.040
- Henkes, G. A., Passey, B. H., Grossman, E. L., Shenton, B. J., Yancey, T. E., and Pérez-Huerta, A. (2018). Temperature Evolution and the Oxygen Isotope Composition of Phanerozoic Oceans from Carbonate Clumped Isotope Thermometry. *Earth Planet. Sci. Lett.* 490, 40–50. doi:10.1016/j.epsl.2018.02.001
- Héroux, Y., Chagnon, A., and Bertrand, R. (1979). Compilation and Correlation of Major thermal Maturation Indicators. *AAPG Bull.* 63, 2128–2144. doi:10.1306/2f9188f1-16ce-11d7-8645000102c1865d
- Hill, R. J., Tang, Y., and Kaplan, I. R. (2003). Insights into Oil Cracking Based on Laboratory Experiments. *Org. Geochem.* 34, 1651–1672. doi:10.1016/s0146-6380(03)00173-6
- Hunt, J. M. (1996). *Petroleum Geology and Geochemistry*. 2nd edition. New York: Freeman and Company, 144p.
- Huntington, K. W., Eiler, J. M., Affek, H. P., Guo, W., Bonifacie, M., Yeung, L. Y., et al. (2009). Methods and Limitations of 'clumped' CO<sub>2</sub> isotope (Δ47) Analysis by Gas-Source Isotope Ratio Mass Spectrometry. *J. Mass. Spectrom.* 44 (9), 1318–1329. doi:10.1002/jms.1614
- Jacob, H. (1989). Classification, Structure, Genesis and Practical Importance of Natural Solid Oil Bitumen ("migrabitumen"). *Int. J. Coal Geology.* 11, 65–79. doi:10.1016/0166-5162(89)90113-4
- Jiang, L., Worden, R. H., Cai, C., Li, K., Xiang, L., Cai, L., et al. (2014). Dolomitization of Gas Reservoirs: The Upper Permian Changxing and Lower Triassic Feixianguan Formations, Northeast Sichuan Basin, China. *J. Sediment. Res.* 84, 792–815. doi:10.2110/jsr.2014.65
- Katz, B. J., and Lin, F. (2021). Consideration of the Limitations of thermal Maturity with Respect to Vitrinite Reflectance, Tmax, and Other Proxies. *Bulletin* 105, 695–720. doi:10.1306/09242019261
- Kinley, T. J., Cook, L. W., Breyer, J. A., Jarvie, D. M., and Busbey, A. B. (2008). Hydrocarbon Potential of the Barnett Shale (Mississippian), Delaware Basin, West Texas and southeastern New Mexico. *Bulletin* 92, 967–991. doi:10.1306/03240807121
- Li, J., Xie, Z., Dai, J., Zhang, S., Zhu, G., and Liu, Z. (2005). Geochemistry and Origin of Sour Gas Accumulations in the Northeastern Sichuan Basin, SW China. *Org. Geochem.* 36, 1703–1716. doi:10.1016/j.orggeochem.2005.08.006
- Li, P., Zou, H., Hao, F., Yu, X., Wang, G., and Eiler, J. M. (2020). Using Clumped Isotopes to Determine the Origin of the Middle Permian Qixia Formation Dolostone, NW Sichuan Basin, China. *Mar. Pet. Geology.* 122, 104660. doi:10.1016/j.marpetgeo.2020.104660
- Li, P., Zou, H., Yu, X., Hao, F., and Wang, G. (2021). Source of Dolomitizing Fluids and Dolomitization Model of the Upper Permian Changxing and Lower Triassic Feixianguan Formations, NE Sichuan Basin, China. *Mar. Pet. Geology.* 125, 104834. doi:10.1016/j.marpetgeo.2020.104834
- Liu, S., Yang, Y., Deng, B., Zhong, Y., Wen, L., Sun, W., et al. (2021). Tectonic Evolution of the Sichuan Basin, Southwest China. *Earth-Science Rev.* 213, 103470. doi:10.1016/j.earscirev.2020.103470
- Lloyd, M. K., Ryb, U., and Eiler, J. M. (2018). Experimental Calibration of Clumped Isotope Reordering in Dolomite. *Geochimica et Cosmochimica Acta* 242, 1–20. doi:10.1016/j.gca.2018.08.036
- Luo, B., Wen, L., Zhang, Y., Xie, C., Cao, J., Xiao, D., et al. (2020b). Differential Gas Accumulation Process of the Middle Permian Qixia Formation, Northwestern Sichuan Basin. *Oil Gas Geology.* 41, 393–406. (in Chinese with English abstract).
- Luo, Q., Fariborz, G., Zhong, N., Wang, Y., Qiu, N., Skovsted, C. B., et al. (2020a). Graptolites as Fossil Geo-Thermometers and Source Material of Hydrocarbons: An Overview of Four Decades of Progress. *Earth-Science Rev.* 200, 103000. doi:10.1016/j.earscirev.2019.103000
- Ma, Y., Guo, X., Guo, T., Huang, R., Cai, X., and Li, G. (2007). The Puguang Gas Field: New Giant Discovery in the Mature Sichuan Basin, Southwest China. *Bulletin* 91, 627–643. doi:10.1306/11030606062
- Mukhopadhyay, P. K. (1994). "Vitrinite Reflectance as Maturity Parameter," in *Vitrinite reflectance as a maturity parameter: Applications and limitations*. Editors P. K. Mukhopadhyay and W. G. Dow (Washington, DC: American Chemical Society Symposium Series), 570, 1–24. doi:10.1021/bk-1994-0570.ch001
- Pan, L., Shen, A., Zhao, J.-x., Hu, A., Hao, Y., Liang, F., et al. (2020). LA-ICP-MS U-Pb Geochronology and Clumped Isotope Constraints on the Formation and Evolution of an Ancient Dolomite Reservoir: The Middle Permian of Northwest Sichuan Basin (SW China). *Sediment. Geology.* 407, 105728. doi:10.1016/j.sedgeo.2020.105728
- Passey, B. H., and Henkes, G. A. (2012). Carbonate Clumped Isotope Bond Reordering and Geospeedometry. *Earth Planet. Sci. Lett.* 351–352, 223–236. doi:10.1016/j.epsl.2012.07.021
- Qiu, N., Chang, J., Zuo, Y., Wang, J., and Li, H. (2012). Thermal Evolution and Maturation of Lower Paleozoic Source Rocks in the Tarim Basin, Northwest China. *Bulletin* 96, 789–821. doi:10.1306/09071111029
- Reiners, P. W. (2005). Zircon (U-Th)/He Thermochronometry. *Rev. Mineralogy Geochem.* 58, 151–179. doi:10.2138/rmg.2005.58.6
- Ryb, U., and Eiler, J. M. (2018). Oxygen isotope composition of the Phanerozoic ocean and a possible solution to the dolomite problem. *Proc. Natl. Acad. Sci. USA*, 115, 6602–6607. doi:10.1073/pnas.1719681115
- Schmidt, J. S., Menezes, T. R., Souza, I. V. A. F., Spigolon, A. L. D., Pestilho, A. L. S., and Coutinho, L. F. C. (2019). Comments on Empirical Conversion of Solid Bitumen Reflectance for thermal Maturity Evaluation. *Int. J. Coal Geology.* 201, 44–50. doi:10.1016/j.coal.2018.11.012
- Stach, E., Mackowsky, M. T., Taylor, G. H., Chandra, D., Teichmüller, M., and Teichmüller, R. (1982). *Stach's text book of coal petrology*. 3rd ed. Stuttgart: Borntraeger, 535.
- Stolper, D. A., and Eiler, J. M. (2015). The Kinetics of Solid-State Isotope-Exchange Reactions for Clumped Isotopes: a Study of Inorganic Calcites and Apatites from Natural and Experimental Samples. *Am. J. Sci.* 315, 363–411. doi:10.2475/05.2015.01
- Sun, Y., Joachimski, M. M., Wignall, P. B., Yan, C., Chen, Y., Jiang, H., et al. (2012). Lethally Hot Temperatures during the Early Triassic Greenhouse. *Science* 338, 366–370. doi:10.1126/science.1224126
- Sweeney, J. J., and Burnham, A. K. (1990). Evaluation of a Simple Model of Vitrinite Reflectance Based on Chemical Kinetics. *Aapg Bull.* 74, 1559–1570.
- Wood, D. A. (2018). Kerogen Conversion and thermal Maturity Modelling of Petroleum Generation: Integrated Analysis Applying Relevant Kerogen Kinetics. *Mar. Pet. Geology.* 89, 313–329. doi:10.1016/j.marpetgeo.2017.10.003
- Yamada, R., Murakami, M., and Tagami, T. (2007). Statistical Modelling of Annealing Kinetics of Fission Tracks in Zircon; Reassessment of Laboratory Experiments. *Chem. Geology.* 236, 75–91. doi:10.1016/j.chemgeo.2006.09.002
- Yu, Y., Li, P., Guo, R., Zhao, Y., Li, S., and Zou, H. (2021). Upwelling-induced Organic Matter Enrichment of the Upper Permian Dalong Formation in the Sichuan Basin, SW China and its Paleoenvironmental Implications. *Palaeogeogr. Palaeoclimatol. Palaeoecol.* 576, 110510. doi:10.1016/j.palaeo.2021.110510
- Zhai, G. M. (1989). *Petroleum Geology of China*, Vol. 10. Beijing: Petroleum Industry Press. (in Chinese).
- Zhu, C., Hu, S., Qiu, N., Rao, S., and Yuan, Y. (2016). The thermal History of the Sichuan Basin, SW China: Evidence from the Deep Boreholes. *Sci. China Earth Sci.* 59, 70–82. doi:10.1007/s11430-015-5116-4
- Zhu, G., Milkov, A. V., Chen, F., Weng, N., Zhang, Z., Yang, H., et al. (2018). Non-cracked Oil in Ultra-deep High-Temperature Reservoirs in the Tarim basin, China. *Mar. Pet. Geology.* 89, 252–262. doi:10.1016/j.marpetgeo.2017.07.019
- Zuo, Y., Qiu, N., Zhang, Y., Li, C., Li, J., Guo, Y., et al. (2011). Geothermal Regime and Hydrocarbon Kitchen Evolution of the Offshore Bohai Bay Basin, North China. *Bulletin* 95, 749–769. doi:10.1306/09271010079

**Conflict of Interest:** JD was employed by SINOPEC Exploration Company.

The remaining authors declare that the research was conducted in the absence of any commercial or financial relationships that could be construed as a potential conflict of interest.

**Publisher's Note:** All claims expressed in this article are solely those of the authors and do not necessarily represent those of their affiliated organizations, or those of the publisher, the editors and the reviewers. Any product that may be evaluated in this article, or claim that may be made by its manufacturer, is not guaranteed or endorsed by the publisher.

Copyright © 2021 Li, Duan, Cheng and Zou. This is an open-access article distributed under the terms of the Creative Commons Attribution License (CC BY). The use, distribution or reproduction in other forums is permitted, provided the original author(s) and the copyright owner(s) are credited and that the original publication in this journal is cited, in accordance with accepted academic practice. No use, distribution or reproduction is permitted which does not comply with these terms.